Acta Neuropathologica Communications

RESEARCH

Open Access

Density and entropy of immune cells within the tumor microenvironment of primary tumors and matched brain metastases

Markus Kleinberger[1,2], Didem Çifçi[3], Christina Paiato[1], Erwin Tomasich[1,2], Maximilian J Mair[1,2], Ariane Steindl[1,2], Zoltán Spiró[1,2,4], Zunamys I. Carrero[3], Luzia Berchtold[1,2,5], Johannes Hainfellner[6,7], Leonhard Müllauer[8], Gerwin Heller[1,2], Matthias Preusser[1,2], Jakob Niklas Kather[3,9,10] and Anna Sophie Berghoff[1,2*]

Abstract

Background Tumor-infiltrating lymphocytes (TILs) and tumor-associated macrophages (TAMs) have increasingly been reported to impact the brain metastatic process of solid tumors. However, data on intra-individual differences between primary tumor and brain metastasis (BM), as well as their correlation with clinical outcome parameters, is scarce.

Methods We retrospectively identified patients who received resection of the primary tumor and BM between 01/1990 and 10/2022. Density quantification of TAMs ($CD68^+$, $CD163^+$) and TILs ($CD3^+$, $CD8^+$, $CD45RO^+$, $FOXP3^+$) was performed by immunohistochemical staining of matched tumor tissue samples. Images were processed with QuPath software and heterogeneity of generated heatmaps was measured by Shannon Entropy. Time-to-BM (TTBM) was defined as the time from diagnosis of the primary tumor until the first diagnosis of BM.

Results In total, 104 patients (46.2% female; median age 57.3 years at BM diagnosis) were included: 78/104 (75%) non-small cell lung cancer, 18/104 (17%) breast cancer, 8/104 (8%) renal cell carcinomas. Densities of $CD3^+$ ($p<0.001$) and $CD8^+$-TILs ($p<0.001$) were higher in primary tumor samples, while $CD68^+$ ($p=0.035$) and $CD163^+$-TAM densities ($p<0.001$) were higher in the matched BM. Higher $CD3^+$, $CD8^+$-TILs and $CD163^+$-TAMs densities in primary tumors were associated with shorter TTBM ($p=0.005$, $p=0.015$ and $p=0.006$, respectively). Higher entropies of $CD3^+$ ($p<0.001$) and $FOXP3^+$ ($p=0.011$) TILs were observed in primary tumors compared to BM. Longer TTBM was associated with higher entropy of $FOXP3^+$ TILs ($p=0.024$) and lower entropy in $CD163^+$ TAMs ($p=0.039$). No significant associations of immune cell densities or entropies with OS after BM diagnosis were found.

Discussion By utilizing a unique cohort of matched primary tumor and BM tissue samples, we could demonstrate higher TIL densities in primary tumors and higher TAM densities in BM, respectively. Higher cell densities of $CD3^+$, $CD8^+$-TILs and $CD163^+$-TAMs in primary tumors were associated with shorter TTBM, while a larger difference between $CD3^+$ and $CD8^+$ densities between primary tumor and BM was associated with longer TTBM. These findings highlight the potential of targeting TAMs as a therapeutic strategy to mitigate the development of brain metastases.

*Correspondence:
Anna Sophie Berghoff
anna.berghoff@meduniwien.ac.at

Full list of author information is available at the end of the article

© The Author(s) 2025. **Open Access** This article is licensed under a Creative Commons Attribution-NonCommercial-NoDerivatives 4.0 International License, which permits any non-commercial use, sharing, distribution and reproduction in any medium or format, as long as you give appropriate credit to the original author(s) and the source, provide a link to the Creative Commons licence, and indicate if you modified the licensed material. You do not have permission under this licence to share adapted material derived from this article or parts of it. The images or other third party material in this article are included in the article's Creative Commons licence, unless indicated otherwise in a credit line to the material. If material is not included in the article's Creative Commons licence and your intended use is not permitted by statutory regulation or exceeds the permitted use, you will need to obtain permission directly from the copyright holder. To view a copy of this licence, visit http://creativecommons.org/licenses/by-nc-nd/4.0/.

Introduction

The tumor microenvironment (TME) represents an ecosystem consisting of a variety of malignant and non-malignant cells, organized through highly complex cell-cell interactions, subcellular communication and crosstalk [1]. Intra-tumoral immune cells like tumor-infiltrating lymphocytes (TILs) or tumor-associated macrophages (TAMs) are the main effector cells of the inflammatory microenvironment [2, 3]. Particularly in the face of novel treatment options the presence of specific immune cell subtypes within the unique TME of brain metastases has demonstrated associations with higher intracranial response rates to immune checkpoint inhibitors (ICI) [4].

However, concerning the high heterogeneity within the TME additional information about the spatial distribution is essential to sufficiently analyze immune cell infiltration pattern and to put them into perspective with biological traits [5]. Besides the intratumoral genetic and epigenetic characteristics the localization and co-localization within the TME are pivotal for cellular crosstalk of cancer and immune effector cells [6, 7]. Although previous studies addressed the characterization of the TME in high-level resolution, in-depth information on differences between tumor sites is missing due to the infrequent availability of more than one tumor sample from the same patient [8–14].

In the current study, we aimed to improve the understanding of intrapersonal differences in the TME between primary tumors and matched brain metastases (BM) by using a unique cohort of 104 patients with matched tissue samples. While this study primarily focuses on the descriptive and methodological aspects of TME characterization, we also explored associations with clinical parameters, including time-to-brain metastasis (TTBM), to provide initial insights into potential prognostic implications.

Materials and methods

Patient cohort

Patients diagnosed with histologically confirmed and intracranial metastasized non-small cell lung cancer (NSCLC), breast cancer (BC) and renal cell carcinoma (RCC) were retrospectively identified from the Vienna Brain Metastasis Registry. Patients with tissue samples of the primary tumor and BM via tumor resection or excision between 01/1990 and 12/2022 at the Medical University of Vienna were included. Patients with insufficient formalin-fixed and paraffin-embedded (FFPE) tumor samples (e.g., fine needle aspiration) were excluded. FFPE specimens available for scientific purposes were obtained from the Department of Pathology and Department of Neurology, Division of Neuropathology and Neurochemistry. Clinical data were extracted from the Vienna Brain Metastasis Registry and electronic patient charts. This retrospective exploratory study was approved by the Ethics Committee of the Medical University of Vienna (EC approvals no. 1692/2022, 1895/2022) in accordance with the Declaration of Helsinki. Due to the retrospective nature of the study the necessity of written informed consent was waived by the competent authorities. An illustrated workflow is presented in Fig. 1.

Immunohistochemistry

FFPE tumor blocks of primary and matched BM were prepared by cutting in 4 µm thick sections. Consecutive immunohistochemical staining was performed on a Ventana Benchmark ULTRA machine (Roche Diagnostics, Rotkreuz, Switzerland) by using the following antibodies: CD3 (SP7, Epredia, US), CD8 (C8/144B, Dako, US), CD45RO (UCHL1, Dako, US), FOXP3 (206D, BioLegend, US), CD68 (KP1, Dako, US), CD163 (MRQ-26, Cell Marque, US) (Fig. 2). $CD3^+$ cells were used to assess total T cells, $CD8^+$ cells for cytotoxic T lymphocytes (CTLs), and $FOXP3^+$ cells for regulatory T cells (T_{regs}). In addition, $CD68^+$ and $CD163^+$ cells were used to assess tumor-associated macrophages (TAMs), with CD68 marking pan-macrophages and CD163 indicating a subset of alternatively activated (M2-like) macrophages. CD45RO was used to assess memory T cells. These markers were selected based on their well-established roles in immune response characterization in cancer.

Heat-induced antigen retrieval was done by incubating with Tris-EDTA-based Cell Conditioning 1 (CC1) buffer (Roche Diagnostics, Rotkreuz, Switzerland) for all used antibodies. The protein expression was visualized using the UltraView DAB IHC Detection Kit (Ventana) and counterstained with Hematoxylin and Bluing Reagent (Ventana). The used protocol including the well-established specific conditions for each antibody is provided in Supplementary Table 1.

Image analysis

Stained slides were digitalized by using NanoZoomer S60 slide scanner (Hamamatsu Photonics, Hamamatsu City, Japan) with 40x magnification. For further analysis, QuPath software was used as previously described [15]. The following steps were performed and quality-controlled by a pathology-trained physician to avoid interobserver variability. Briefly, whole slide images of the same entity were loaded into batches and underwent semi-automatic tissue detection. Artifacts such as anthracotic pigments or hemosiderin, as well as healthy adjacent tissue were carefully cropped to avoid affecting accuracy of automatic processing (Supplementary Fig. 1). For cell detection, an automated detection algorithm in QuPath was used, with thresholds individually optimized for each staining. Therefore, at least one digital fraction of the

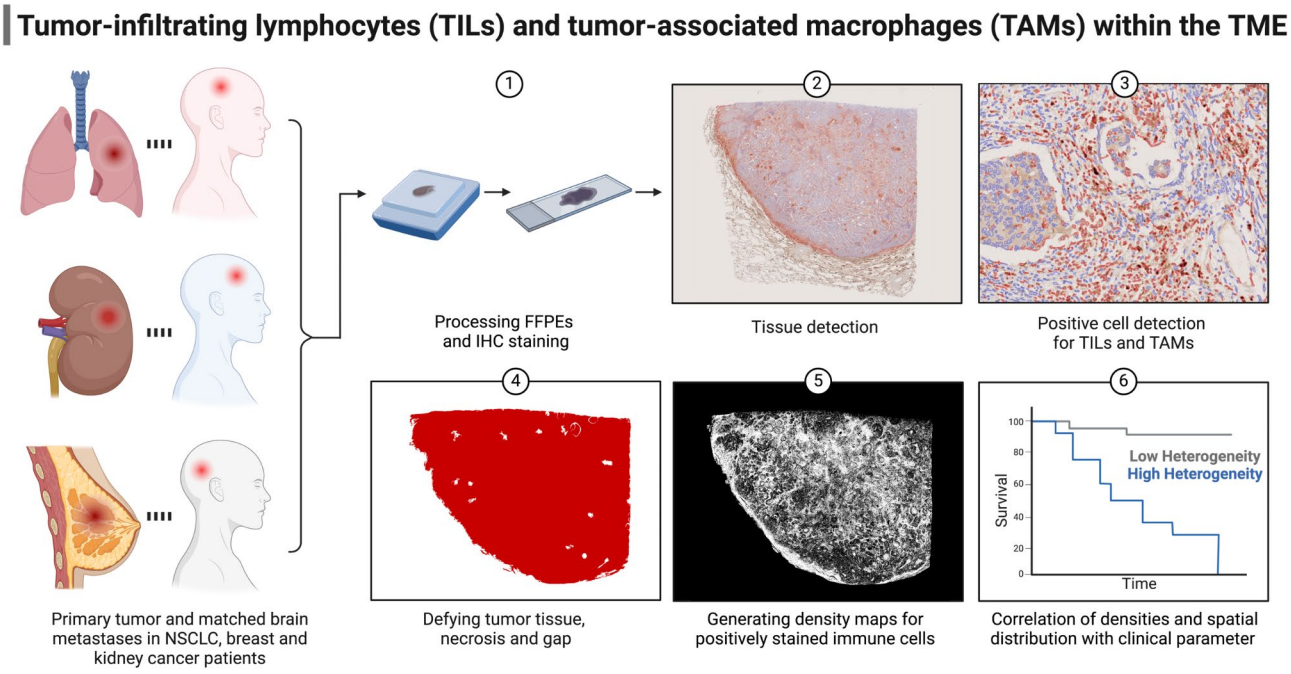

Fig. 1 Workflow of data acquisition. (**1**) FFPE tumor tissue samples were cut and stained with IHC for TIL and TAM marker. (**2**) After scanning digitalized slides were further analyzed with QuPath. Tissue was detected automatically, and false positive contamination was removed manually. (**3**) Positive cell detection for tissue annotations. (**4**) Pixel classification for regions of interest (tumor, necrosis, gap). Tumor maps generated and exported by automatic script. (**5**) Generating density maps for positive cells. (**6**) Entropy indices were calculated by using density and tumor map. Shannon entropy and cell densities [cells/mm^2] were correlated with patient characteristics and outcome parameters. Graphical abstract was designed with Biorender

included whole slide images was assembled to one collage to represent fractions of all included slides. Cellular detections were subsequently performed on this collage, adapted, applied to all included images which were then reviewed and verified. Identical cellular detection settings were applied consistently across all slides for each marker. After positive cell detection the tissue area was segmented into "gap" (areas devoid of tissue), "tumor" (including stromal and epithelial tumor tissue), and "necrosis" by using the same image collage. Further stratification into stromal and epithelial tumor compartments was not conducted, as this level of granularity reduced the accuracy of the semi-automatic tissue classification. After visual quality control settings for tissue separation were then applied to all images. Heatmaps showing positive cells and tumor maps were exported automatically by a Groovy script in QuPath. Ultimately, measurements of density by positive cells per mm [2] tumor were exported.

Shannon entropy

Prior to further analysis, the tumor maps were subjected to Gaussian blurring to refine the tumor region annotations. A Gaussian kernel with a sigma value of 15 pixels was applied to each tumor map. The selection of the sigma value was based on qualitative assessment through visual inspection to achieve a balance between smoothing the tumor boundaries while retaining their essential characteristics. Binary tumor masks were derived from the Gaussian-blurred tumor maps through a thresholding operation. The threshold value was set to the 75th percentile of pixel intensity values within each blurred tumor map. Pixels with intensities exceeding this threshold were assigned a value of 1, representing tumorous regions, while those below were assigned a value of 0, representing non-tumorous regions. This operation effectively segmented and extracted only the regions of interest, i.e., the tumor regions, from the original density heatmaps.

Shannon entropy was computed for the extracted tumorous regions within the density heatmaps to quantify the heterogeneity of tumor density. Shannon entropy (H) is a statistical measure of randomness or uncertainty within a given region [16]. For each isolated tumor region, the entropy was calculated using the formula:

$$H(x) = -\sum_{i=1}^{n} p(x_i)\, log_2 p(x_i)$$

n is the number of discrete intensity levels in the density values within the tumor region, and $p(x_i)$ represents the probability of each intensity level occurring within the region. The Shannon entropy thus provided a numerical representation of the spatial heterogeneity of tumor density within each tumor region (see Supplementary Fig. 8).

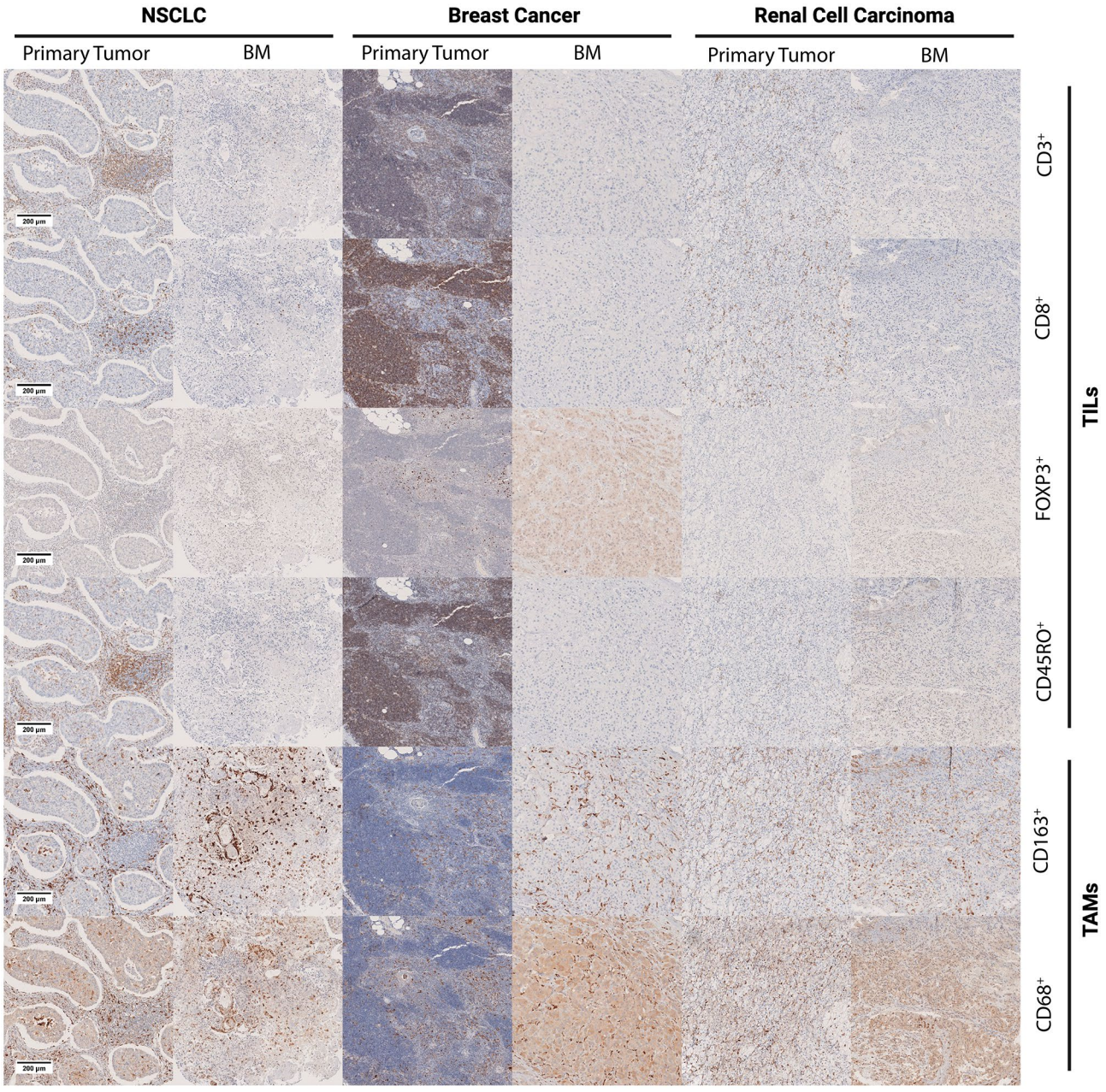

Fig. 2 Immunohistochemical staining of TILs and TAMs in primary tumor and matched brain metastasis

Statistical analysis

Patient characteristics, cell densities and entropy indices are given as absolute numbers, percentage, median and range. Cell densities were measured in number of positive stained cells per mm [2]. To accommodate variations across different staining groups and to ensure consistency of entropy values across all cancer types, the calculated entropy values underwent additional normalization through min-max normalization. This technique standardized the Shannon entropy index values within each staining group to a range of 0 (low heterogeneity) to 1 (high heterogeneity). This step ensured that the entropy values were tailored to the staining groups facilitating comparisons across diverse cancer types. Difference in cell densities and Shannon entropy between primary tumors and matched BM are calculated by subtraction for all immune cell subpopulations. Time-to-BM (TTBM) is measured between histologically confirmed diagnosis of primary tumor and BM. In case the BM is diagnosed prior to the primary tumor TTBM is zero. Patients with diagnosis of BM within 2 months after primary tumor diagnosis are considered as synchronously diagnosed in accordance with previous studies [17, 18]. Overall survival after BM is calculated between the

date of histological diagnosis of the BM and death. To account for the treatment administered in-between and the differences among entities, we applied a linear mixed model including these variables and the sample origin as a fixed effect with interaction terms and a random effect for each patient. In this, as well as the subsequent analyses, we used a square root transformation on the data to meet the normality assumption. Unpaired t-test was then used to test for a statistically significant difference between the squared density and entropy values of primary tumor and BM samples. The association between OS after BM / TTBM and the density/entropy differences were inspected using Cox regression models and the difference in density/entropy as sole predictor variable. To test if the association is irrespective of Graded Prognostic Assessment (GPA), we constructed an additional model with an interaction term. By grouping above vs. below median density/entropy value of the respective immune subtype we generated Kaplan-Meier curves and log-rank test. Results were considered significant at a two-sided p-value < 0.05. As the exploratory analyses within this study are aimed at the generation of hypotheses, no adjustment for multiple testing was applied [19]. However, Bonferroni-Holm correction was additionally used for adjusted testing and presented in the supplementary data. Statistical analysis and data visualization were performed using R 4.2.2 (The R Project for Statistical Computing, Vienna, Austria). The graphical abstract (Fig. 1) was illustrated with Biorender.com.

Results

Patients characteristics

Overall, 104 patients with matched samples of the primary tumor and the BM samples were available: 78/104 (75%) non-small cell lung cancer, 18/104 (17%) breast cancer, 8/104 (8%) renal cell carcinomas. This population comprised of 56/104 males (53.8%) and 48/104 females (46.2%), whereas all breast cancer patients were female. The median age at BM diagnosis was 57 years (range 28–77), with significant differences between entities regarding TTBM (log rank $p < 0.001$, see Supplementary Fig. 9). Prior to BM resection 54/104 (51.9%) received systemic chemotherapy and 6/104 (5.8%) had cranial radiotherapy. ICI was administered to 4/74 (5.4%) NSCLC patients (3/74 prior and 1/74 after BM diagnosis) while none of the included RCC or BC patients received immunotherapy. For detailed information concerning patients' characteristics refer to Table 1.

Difference of cell density and entropy between primary tumor and matched BM

Overall, higher TIL density was found in primary tumors, while BM presented with a higher fraction of TAMs (Fig. 3; Table 2). In detail, using unadjusted paired t-test of squared values of the immune cell densities we observed significantly higher densities of $CD3^+$ (median 589 vs. 63 cells/mm^2, $p < 0.001$) and $CD8^+$ (median 207 vs. 33 cells/mm^2, $p < 0.001$) in primary tumors. In contrast, higher $CD68^+$ (median 866 vs. 1081 cells/mm^2, $p = 0.035$) and $CD163^+$-TAM densities were observed in matched BM (median 444 vs. 811 cells/mm^2, $p < 0.001$). These differences were significant irrespective of applied systemic treatment or entity (all $p < 0.001$). In $CD45RO^+$ ($p = 0.279$) and $FOXP3^+$ ($p = 0.377$) TILs, no significant differences were observed between primary tumors and BM. When adjusted for multiple testing significant differences of cell densities in $CD3^+$ ($p < 0.001$), $CD8^+$ ($p < 0.001$) and $CD163^+$ ($p < 0.001$) prevailed (see Supplementary Table 3).

Overall, higher entropy levels were observed in primary tumors compared to matched BM, arguing for a more heterogeneous infiltration throughout the primary tumor compared to BM (Fig. 4). In detail, significantly higher entropy values in primary tumors were observed for $CD3^+$ (median 0.8 vs. 0.61, $p < 0.001$) and $FOXP3^+$ (median 0.50 vs. 0.41, $p = 0.011$) TILs. When adjusted for multiple testing differences in CD3 + entropy between primary tumor and BM remained significant ($p = 0.0196$, see Supplementary Table 3). No significant difference in TAM entropy levels between primary and matched BM were present. Detailed summary of immune cell densities and entropies are shown in Tables 2 and 3 and graphically in Figs. 3 and 4, as well as in Supplementary Figs. 4–7. Differences regarding the specific tumor entities are additionally illustrated in Supplementary Figs. 2 and 3.

Association of difference in immune cell densities and entropy between primary tumor and BM and time to BM (TTBM)

Next, we aimed to investigate whether the observed differences in TIL and TAM densities and entropies between primary tumor and matched BM are associated with the clinical course of these patients. Twenty-eight patients (26.9%) were synchronously diagnosed with primary tumor and BM. The median TTBM in the non-synchronously diagnosed patients (76/104; 73.1%) was 18.9 months (range 2.4–119.5). In the non-synchronously diagnose population and separated by entity, median TTBM in NSCLC patients was 15.4 months (range 2.4–73.4), 27.6 months in RCC (range 2.8–119.5) and 29.3 (range 13.1–64.6) in BC patients. Of all non-synchronously diagnosed patients 51/82 (62.2%) received systemic treatment between the diagnosis of primary tumor and BM. In treated patients, the median TTBM was 18.6 months (range 0–119.5) and in non-treated patients 13.9 months (range 0.2–73.4; $p = 0.21$).

A difference in $CD3^+$ ($p = 0.005$, HR 1.06, 95% CI: 1.02–1.09), $CD8^+$ ($p = 0.015$, HR 1.06, 95% CI: 1.01–1.11)

Table 1 Clinical and histopathological patient characteristics

	NSCLC ***n*** **= 78 (75%)**	**Breast Cancer** ***n*** **= 18 (17.3%)**	**RCC** ***n*** **= 8 (7.7%)**	**All** ***n*** **= 104 (100%)**
Sex				
male	50 (64.1%)	0	7 (87.5%)	57 (53.8%)
female	28 (35.9%)	18 (100%)	1 (12.5%)	47 (46.2%)
Age diagnosis BM [years]				
median	58.1	46	54.5	57
range	44–77	28–73	44–69	28–77
KPS preoperative (BM)				
median	80	70	75	80
range	40–100	60–100	10–100	10–100
not available	1 (1.3%)	0	0	1 (0.9%)
Graded Prognostic Assessment				
median	2.5	2	2	2.5
range	0.5-4	1–4	1–3	0.5-4
Year of BM diagnosis				
1990–2000	15 (19.2%)	3 (16.7%)	5 (62.5%)	23 (22.1%)
2001–2010	33 (42.3%)	6 (33.3%)	3 (37.5%)	42 (40.4%)
2011–2020	30 (38.5%)	9 (50.0%)	0	39 (37.5%)
Immunohistochemistry				
ER positive		8 (44.4%)		8 (7.7%)
PR positive		4 (22.2%)		4 (3.8%)
HER2 positive		3 (16.7%)		3 (2.9%)
Histopathology				
Adenocarcinoma	61 (78.3%)			61 (58.7%)
Squamous Cell Carcinoma	14 (17.9%)			14 (13.5%)
Large Cell Carcinoma	3 (3.8%)			3 (2.9%)
Ductal		15 (83.3%)		15 (14.4%)
Lobular		2 (11.1%)		2 (1.9%)
Adenocystic		1 (5.6%)		1 (0.9%)
Clear Cell Carcinoma			8 (100%)	8 (7.7%)
Subtypes				
Luminal		8 (44.4%)		8 (7.7%)
HER2		1 (5.6%)		1 (0.9%)
TNBC		9 (50%)		9 (8.6%)
Grading				
G1	1 (1.3%)	1 (5.6%)	0	2 (1.9%)
G2	23 (29.5%)	5 (27.7%)	5 (62.5%)	33 (31.7%)
G3	26 (33.4%)	12 (66.7%)	0	38 (36.6%)
G4	1 (1.3%)	0	2 (25.0%)	3 (2.9%)
unknown	27 (34.5%)	0	1 (12.5%)	28 (26.9%)
Staging at BM diagnosis				
Synchronous BM	26 (33.4%)	1 (5.6%)	1 (12.5%)	28 (26.9%)
Multiple BM	22 (28.2%)	8 (44.4%)	1 (12.5%)	31 (29.8%)
Concomitant extracranial metastasis	19 (24.4%)	12 (66.7%)	7 (87.5%)	38 (36.6%)
Neoadjuvant BM therapy				
Chemotherapy	33 (42.3%)	16 (88.9%)	5 (62.5%)	54 (51.9%)
Radiotherapy	5 (6.4%)	0	1 (12.5%)	6 (5.8%)
Time-to-BM median [weeks]				
median	44.8	126.2	118.1	57.1
range	0-320.0	0-281.3	3.6-520.6	0-520.6

Table 1 (continued)

	NSCLC *n* = 78 (75%)	Breast Cancer *n* = 18 (17.3%)	RCC *n* = 8 (7.7%)	All *n* = 104 (100%)
Overall survival				
median	62.4	28.0	61.7	53.7
from BM diagnosis range	3.0-787.1	0.9-164.4	1.9-262.9	0.9-787.1
[weeks] censored	12 (15.4%)	3 (16.7%)	0	15 (14.4%)

KPS: Karnofsky Performance score, NA: Not applicable

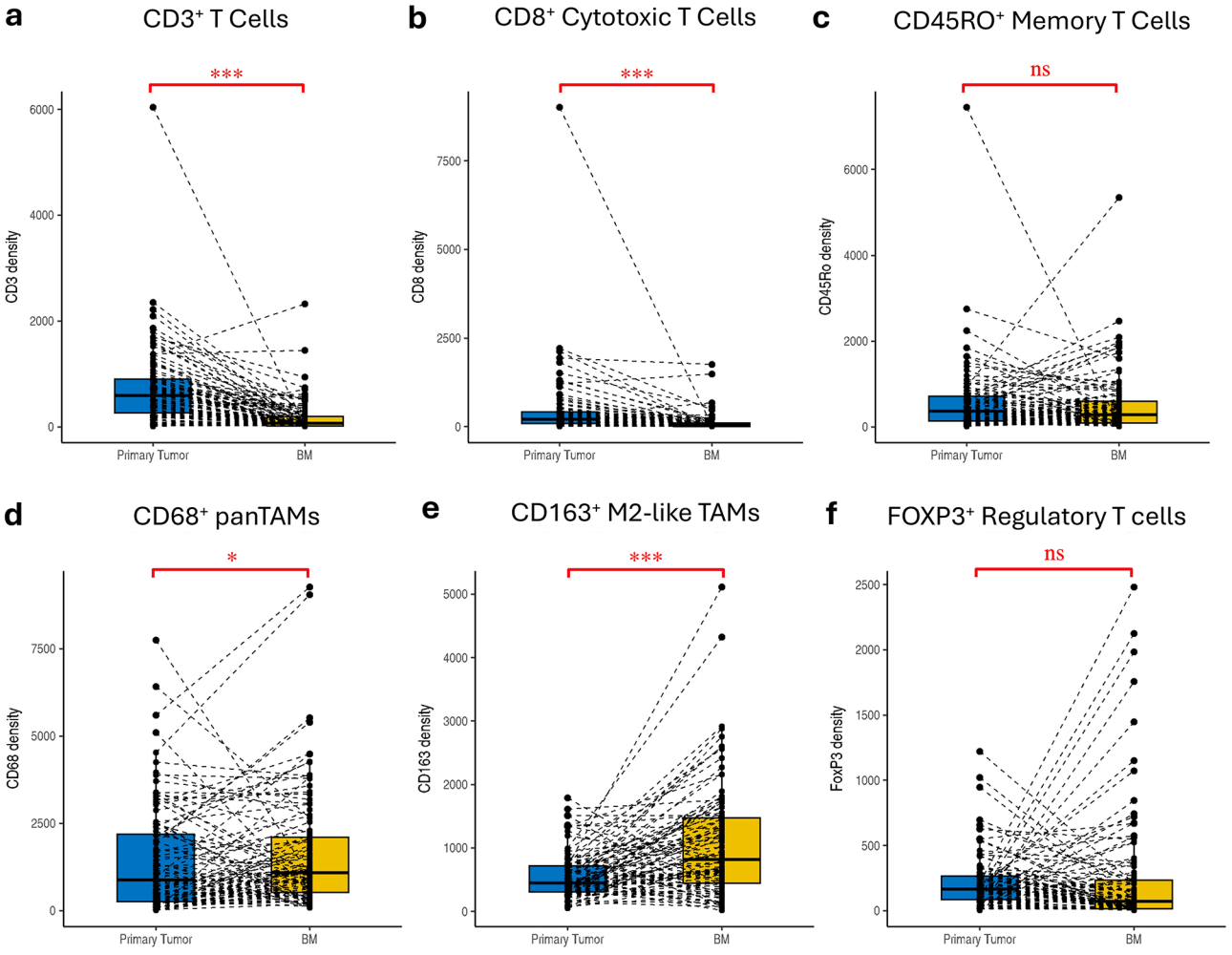

Fig. 3 Differences in immune cell densities between primary tumor and matched brain metastasis (BM). Boxplots indicating significantly higher cell densities [cells/mm2] of (**a**) CD3 + TILs (total TCR + lymphocytes; $p < 0.001$) and (**b**) CD8 + cytotoxic TILs (CD8 + T lymphocytes; $p < 0.001$) in primary tumors compared to brain metastasis (BM). Significantly higher cell densities were found in BM compared to primary tumors regarding (**d**) CD68 + TAMs (pan-macrophages; $p = 0.035$) and (**e**) CD163 + M2-like TAMs (alternatively activated macrophages; $p < 0.001$). No significant differences were found in (**c**) CD45RO + memory T cells ($p = 0.3$) and (**f**) FOXP3 + regulatory T cells (Tregs, $p = 0.377$). ***$p < 0.001$; **$p < 0.01$; *$p < 0.05$; ns . non significant

and CD163⁺ ($p = 0.007$, HR 1.05, 95% CI: 1.01–1.09) but not for CD68⁺ ($p = 0.5$), FOXP3⁺ ($p = 0.4$) or CD45RO⁺ ($p = 0.5$) cell densities between primary tumor and matched BM showed significant positive associations with TTBM. Higher immune cell densities in primary tumors of CD3⁺ ($p = 0.005$, HR 1.06, 95% CI: 1.02–1.09), CD8⁺ TILs ($p = 0.015$, HR 1.06, 95% CI: 1.01–1.11) and CD163⁺-TAMs were associated with shorter TTBM ($p = 0.007$, HR 1.05, 95% CI: 1.01–1.09). Using median cell density of the respective immune cell subtype as cut-off Kaplan-Meier and log-rank test demonstrated significantly shorter TTBM in CD163⁺ density of primary tumor above compared to below median ($p < 0.001$, Supplementary Fig. 10).

Heterogeneity of primary tumors showed positive association with FOXP3⁺ TILs ($p = 0.024$, HR 0.06, 95% CI:

Table 2 Immune cell densities and entropy values (raw values)

			TAMs		TILs			
Cell densities [cell/mm²]			**CD68**	**CD163**	**CD3**	**CD8**	**FOXP3**	**CD45RO**
Overall	Primary	median	866.0	443.9	589.3	207.4	162.9	361.2
		range	3.8-7738.9	51.1-1785.5	2.5-6037.9	2.3-9005.4	2.2-1222.3	8.3-7449.2
	BM	median	1081.0	810.9	62.7	33.4	68.9	282.8
		range	79.3–9261.0	14.3-5109.6	0.4-2322.3	0.0-1758.5	1.5-2480.7	2.6-5341.1
NSCLC	Primary	median	866.0	472.5	639.8	1989.0	165.7	439.4
		range	3.8-6417.6	65.7-1785.5	26.7-2347.9	10.5-1516.8	13.0-1021.2	8.8-2747.0
	BM	median	1047.5	775.9	66.4	26.3	66.9	344.1
		range	79.3-9261.0	14.3-2879.8	0.5-2322.3	0.5-1486.2	1.5-2480.7	2.6-5341.1
BC	Primary	median	306.3	300.6	360.7	388.0	151.1	160.0
		range	98.9-7738.9	51.1-1359.1	2.5-6037.9	2.3-9005.4	2.2-1222.3	8.3-7449.2
	BM	median	961.5	978.7	22.6	32.2	55.2	93.2
		range	237.6-4483.2	155.6-2752.5	5.8-158.9	1.6-135.4	5.7-1757.4	6.7-1917.5
RCC	Primary	median	1613.4	575.3	490.1	540.2	76.0	142.4
		range	425.7-2163.8	238.3-988.7	72.3-1374.1	69.2-2206.0	11.9-945.5	43.0-671.1
	BM	median	1928.8	1468.0	181.9	169.2	92.8	199.8
		range	871.3-5520.9	447.6-5109.6	11.4-1441.6	0.0-1758.5	6.3-673.4	49.9-2470.4
Shannon Entropy [index]			**CD68**	**CD163**	**CD3**	**CD8**	**FOXP3**	**CD45RO**
Overall	Primary	median	0.43	0.51	0.42	0.24	0.34	0.34
		range	0.0–1.0	0.12–0.77	0.11-1.0	0.0–1.0	0.00–1.0	0.06–0.81
	BM	median	0.44	0.67	0.31	0.19	0.27	0.38
		range	0.09–0.82	0.0–1.0	0.0-0.92	0.0-0.66	0.0–1.0	0.0–1.0
NSCLC	Primary	median	0.45	0.53	0.42	0.23	0.36	0.35
		range	0.11–0.8	0.32–0.77	0.11–0.7	0.0-0.49	0.12–0.64	0.07–0.81
	BM	median	0.46	0.70	0.34	0.19	0.27	0.38
		range	0.09–0.8	0.0-0.94	0.0-0.92	0.05–0.66	0.0–1.0	0.0–1.0
BC	Primary	median	0.23	0.4	0.37	0.25	0.28	0.33
		range	0.0–1.0	0.12–0.67	0.15-1.0	0.0–1.0	0.0–1.0	0.06–0.65
	BM	median	0.31	0.17	0.27	0.15	0.27	0.35
		range	0.09–0.62	0.0-0.79	0.05–0.5	0.08–0.25	0.12–0.87	0.01–0.68
RCC	Primary	median	0.42	0.48	0.56	0.36	0.17	0.18
		range	0.11–0.62	0.32–0.59	0.31–0.72	0.14–0.59	0.08–0.52	0.1–0.43
	BM	median	0.37	0.63	0.37	0.25	0.25	0.31
		range	0.26–0.82	0.54-1.0	0.3–0.74	0.0-0.5	0.1–0.38	0.11–0.72

BC: breast cancer, RCC: renal cell carcinoma, TAMs: Tumor-associated macrophages, TILs: Tumor-infiltrating lymphocytes

0.01–0.69) and a negative association for CD163⁺-TAMs ($p = 0.039$, HR 17.1, 95% CI: 1.16–253) with TTBM. Differences between primary tumor and BM in entropy of CD68⁺-TAMs was associated with TTBM ($p = 0.028$, HR 0.1, 95% CI: 0.01–0.78). Data on synchronously and non-synchronously diagnosed patients are displayed in Supplementary Table 2.

Association of immune cell densities and entropy with OS after BM diagnosis

The differences in TIL and TAM density between the primary tumor and matched BM did not correlate with survival after BM diagnosis (all $p > 0.05$). Further, also the difference in TIL and TAM entropies between primary tumor and matched BM did not correlate with survival after BM diagnosis (all $p > 0.05$). However, when using median values as cut-off CD45RO⁺ density in primary tumor above median (log-rank test $p = 0.014$,

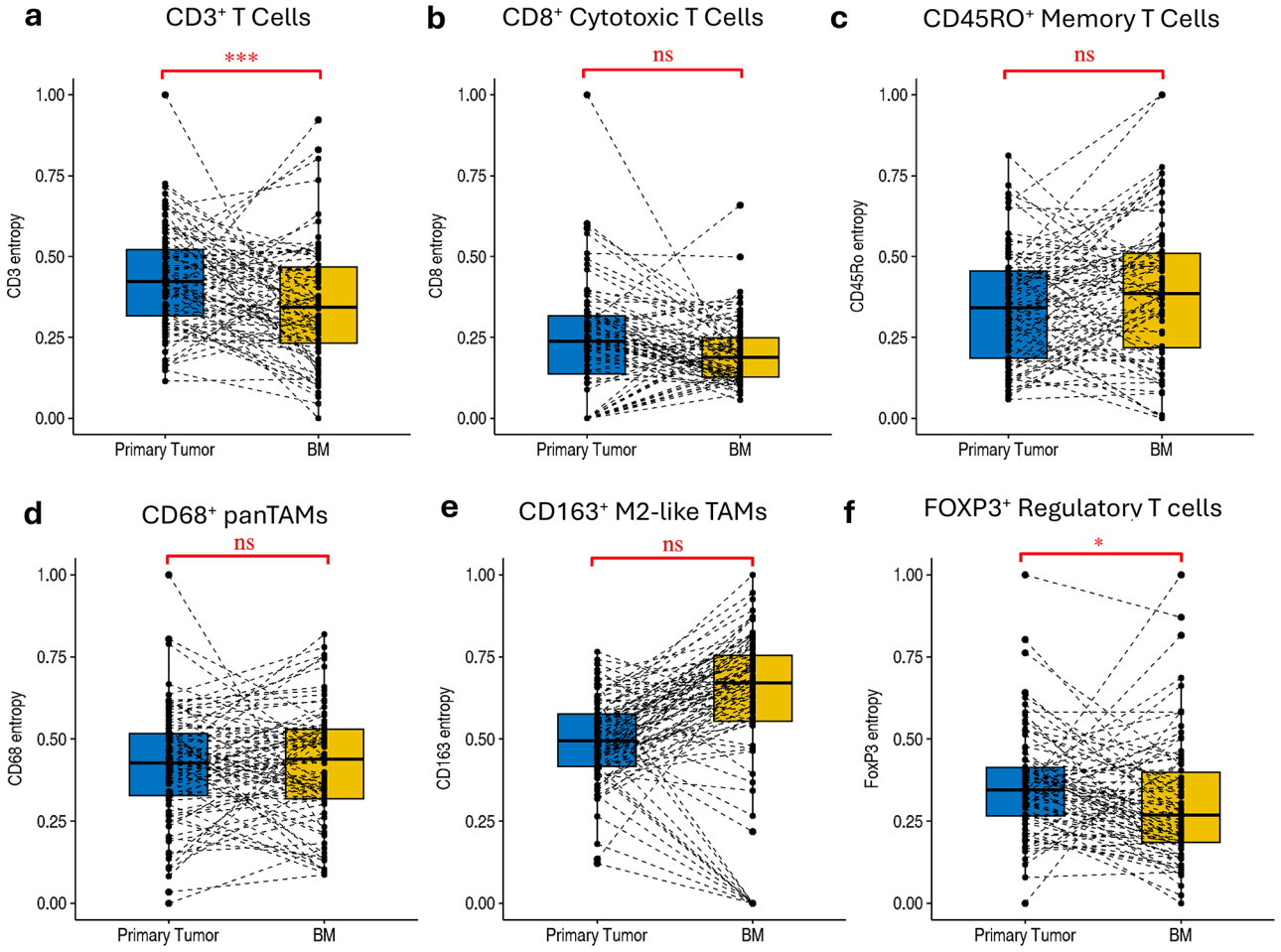

Fig. 4 Differences in immune cell entropies between primary tumor and matched brain metastasis (BM). Boxplots indicating significantly higher entropy values of (**a**) CD3 + TILs (total TCR + lymphocytes; $p < 0.001$) and (**f**) FOXP3 + regulatory T cells (Tregs) in primary tumors compared to brain metastasis (BM; $p = 0.011$). No significant differences were found in (**b**) CD8 + cytotoxic TILs (CD8 + T lymphocytes), (**c**) CD45RO + memory T cells, (**d**) CD68 + TAMs (pan-macrophages) or (**e**) CD163 + M2-like TAMs (alternatively activated macrophages) (all $p > 0.05$). ***$p < 0.001$; **$p < 0.01$; *$p < 0.05$; ns . non significant

Supplementary Fig. 10) and CD163 + TAMs entropy in BM above median showed longer OS (log-rank test $p = 0.041$, Supplementary Fig. 11). Higher GPA was significantly associated with lower overall survival after BM ($p < 0.01$).

Discussion

Changes in the inflammatory microenvironment upon progression are likely to impact the clinical course as well as the response to immune-modulating therapies in patients with solid cancers. Here, we investigated the changes in the inflammatory microenvironment in a unique and large cohort of patients with matched extra- and intracranial tumor tissue. Overall, our data suggest that the composition of the inflammatory microenvironment differs between primary tumors and BM, with primary tumors exhibiting a TIL-dominated infiltration and BM showing a greater presence of TAMs. While these observations indicate a shift in the TME between these sites, further investigation is needed to establish the functional significance of these changes. Further, higher CD3⁺, CD8⁺ TIL and CD163⁺ TAM densities in the primary tumor were associated with shorter TTBM development.

Our data demonstrating higher TAM density in BM compared to matched primary tumors aligns with previous studies suggesting a potentially pro-tumorigenic phenotype of TAMs in BM [8]. These cells may contribute to central nervous system metastasis by modulating vascular integrity and function [20]. Notably, a recent study involving 94 patients with metastatic melanoma reported a positive correlation between higher densities of CD163⁺ TAMs and tumor-associated astrogliosis in BM specimens [21]. In this study, the observed accumulation of CD163⁺ TAMs at the tumor borders suggests a shift toward an anti-inflammatory and tumor-supportive phenotype for this cell subset. Importantly, unlike previous investigations, our study analyzed TAM composition

and density in a particularly large human cohort with matched samples, offering robust evidence to complement preclinical findings. These results underscore the significance of targeting TAMs as a therapeutic strategy, especially in the context of BM development. However, it is crucial to consider the variability of TAMs, as they can exhibit both pro-tumor and anti-tumor phenotypes. Understanding the specific functional roles of TAMs in cancer, particularly in BM by including their phenotypic diversity, will be an important next step in determining whether targeting BM-TAMs could be a viable therapeutic strategy in cancer treatment.

In contrast to TAMs, we could demonstrate significantly lower cell densities of $CD3^+$ and $CD8^+$-TILs in BMs compared to their primary tumor origin. This is in accordance with previous results demonstrating dense infiltration of TILs, particularly CD3 + and CD8 + in primary tumors compared to intracranial metastatic sites [22–24]. Other than macrophages, TILs have recently been analyzed intensively for their cell densities and spatial distribution with solid tumor tissue [25]. Particularly in the face of immune-checkpoint inhibitors utilizing their treatment effects via TILs, the lower densities within BM might explain worse intracranial response rates [26], as well as frequently observed mixed response indicated by shrinking of extracranial lesion, yet intracranial disease progression [27].

To address the challenge of heterogeneity in immune cell infiltration, we employed Shannon entropy derived from heatmaps of tissue slides as an objective metric to quantify spatial heterogeneity. This method enabled the evaluation of immune cell distribution across entire tissue sections in a cost-effective and scalable manner. By avoiding subjective region-specific definitions, such as tumor borders or centers, this approach facilitated uniform and unbiased comparisons across samples while capturing key differences in spatial organization. In contrast, methods that provide deeper insights into the TME, such as multiplex imaging or single-cell analyses, are typically restricted to small tissue regions or require substantial resources, limiting their feasibility for large-scale studies. Our analysis demonstrated that primary tumors exhibited higher entropy levels compared to matched BM, indicating a more heterogeneous distribution of immune cells in primary tumors and a more homogeneous distribution in BM. Specifically, we found that $CD3^+$ and $FOXP3^+$ TILs displayed significantly more heterogeneous infiltration patterns in primary tumors. Furthermore, a more homogeneous distribution of $FOXP3^+$ regulatory T cells in primary tumors was associated with shorter TTBM. In contrast, a more homogeneous distribution of $CD163^+$ TAMs in primary tumors was associated with longer TTBM.

By using subtraction of entropy and cell density between primary tumors and matched BM, we showed that a greater difference in $CD3^+$ and $CD8^+$ TIL densities, as well as in $CD68^+$ entropy values, was associated with longer TTBM. These findings suggest that entropy may serve as a novel method to objectively quantify heterogeneity within the TME, emphasizing the importance of the spatial localization of inflammation.

Overall, these results highlight the potential utility of entropy as a descriptive and quantitative tool for assessing immune cell heterogeneity within the TME. However, it is important to note that this approach provides an artificial and objective measure of distribution patterns rather than a direct replacement for more complex analyses. While entropy offers valuable insights, further research is needed to integrate such metrics into clinical workflows and to fully understand their implications for therapeutic strategies targeting the immune microenvironment.

For correct interpretation of our findings, several limitations of this study must be addressed: Our cohort comprises a relatively large population of matched tumor tissue samples. (i) Samples were recruited over a long period of time, during which anti-cancer treatment standards, particularly the introduction of ICI, have changed significantly. However, we addressed this confounder by including treatment agents and modalities in the multivariable analysis. For RCC, none of the patients received ICI, and in NSCLC, only 4/74 patients received ICI (3 prior to BM diagnosis and 1 after), limiting statistical power for treatment-era comparisons. (ii) The used entropy values only provide information about the heterogeneity of the infiltration yet no specific data about localization. (iii) Additionally, we only included patients who developed BM during the observation period, hence potential patients with longer TTBM exceeding this period were not included. (iv) The retrospective design of our study precludes definite conclusions, (v) as well as the skewed distribution of tumor entities which did not allow us to test for entity-specific correlation or genetic subpopulations. (vi) We utilized IHC for staining, leveraging its widespread clinical applicability, cost-effectiveness, simplicity, and efficiency. While IHC provided valuable insights, the reliance on single-marker analysis limits the ability to fully characterize functional cellular phenotypes, particularly for TAMs. Although $CD68^+$ and $CD163^+$ were used to identify macrophage subsets, these markers alone do not define distinct M1-like (pro-inflammatory) or M2-like (pro-tumorigenic) TAM phenotypes, given the plasticity and heterogeneity of these cells. Future studies employing multiplex imaging or similar advanced techniques are needed to achieve a more comprehensive characterization of TAM subsets and their functional roles within the tumor microenvironment.

Nevertheless, by utilizing this unique cohort of matched primary tumor and BM FFPE whole slide tissue samples, we could address the missing gap of intraindividual spatial and longitudinal changes in the TME of solid tumors.

In summary, we demonstrated higher TIL densities in primary tumors, compared to higher TAM densities in BM. Higher cell densities of $CD3^+$, $CD8^+$-TILs and $CD163^+$-TAMs in primary tumors showed significant associations with shorter TTBM, while a larger difference of $CD3^+$, $CD8^+$ and $CD163^+$ between primary tumor and BM was associated with longer TTBM. Differences in immune cell densities indicate potentially diverting impact of the innate and the adaptive immune system in the process of brain metastatic seeding. Future studies will leverage high-dimensional tissue analysis of this matched sample cohort, to explore the activation and exhaustion states of TILs and the spatial architecture of immune compartments. This will provide a more comprehensive understanding of immune cell interactions and their functional phenotypes. Additionally, integrating multiplexed findings with clinical and transcriptomic data may enable the development of predictive biomarkers for therapeutic responses and shed light on mechanisms driving immune-excluded and immune-inflamed phenotypes in metastatic disease.

Abbreviations

BC	Breast cancer
BM	Brain metastasis
CC1	Cell Conditioning 1
CNS	Central nervous system
CTL	Cytotoxic T Lymphocyte
EC	Ethics committee
FFPE	Formalin-fixed and paraffin-embedded
GMCSF	Granulocyte-macrophage colony-stimulating factor
GPA	Glasgow prognostic score
H	Shannon Entropy
ICI	Immune-checkpoint inhibitor
MCSF	Macrophage colony-stimulating factor
NSCLC	Non-small cell lung cancer
OS	Overall survival
RCC	Renal cell carcinoma
TAM	Tumor-associated macrophages
TIL	Tumor-infiltrating lymphocytes
TME	Tumor microenvironment
TTBM	Time-to-brain metastasis

Supplementary Information

The online version contains supplementary material available at https://doi.org/10.1186/s40478-025-01939-8.

Supplementary Material 1

Supplementary Material 2

Supplementary Material 3

Supplementary Material 4

Supplementary Material 5

Supplementary Material 6

Supplementary Material 7

Supplementary Material 8

Supplementary Material 9

Supplementary Material 10

Supplementary Material 11

Supplementary Material 12

Supplementary Material 13

Supplementary Material 14

Acknowledgements
Not applicable.

Author contributions
M.K. conceived the present idea, designed, and performed the analysis, contributed to sample preparation, interpretated of the results and wrote the manuscript. D.C. performed the analysis of density maps to obtain entropy values and contributed to the interpretation of the results and critical review of the manuscript. C.P. contributed to sample preparation, interpretation of the results and critical review of the manuscript. E.T. contributed to sample preparation, interpretation of the results and critical review of the manuscript. M.J.M. contributed to the imaging analysis with QuPath, the interpretation of the results and critical review of the manuscript. A.S. contributed to obtaining the patient characteristics, the interpretation of the results and critical review of the manuscript. Z.S. contributed to the interpretation of the results and critical review of the manuscript. Z.I.C. helped supervise the project, design the computational framework and the analysis to obtain entropy values and contributed to the interpretation of the results and critical review of the manuscript. L.B. contributed to the statistical analysis, the interpretation of the results and critical review of the manuscript. J.H. contributed to the interpretation of the results and critical review of the manuscript. L.M. contributed to the interpretation of the results and critical review of the manuscript. G.H. contributed to the interpretation of the results and critical review of the manuscript. M.P. helped supervise the project and contributed to interpretation of the results and helped writing the manuscript. J.N.K helped supervise the project, design the computational framework and the analysis to obtain entropy values and contributed to the interpretation of the results and critical review of the manuscript. A.S.B. devised the main conceptual ideas, helped designing the analysis, contributed to the interpretation of the results and helped writing the manuscript. All named authors meet all four criteria for (co)-authorship provided by the Good Scientific Practice guidelines of the Medical University of Vienna. All authors read and approved the final manuscript.

Funding
The financial support by the Austrian Federal Ministry for Digital and Economic Affairs, the National Foundation for Research, Technology and Development and the Christian Doppler Research Association is gratefully acknowledged.

Data availability
No datasets were generated or analysed during the current study.

Declarations

Ethics approval and consent to participate
This study was approved by the Ethics Committees of the Medical University of Vienna (approval no. 1692/2022, 1895/2022).

Consent for publication
Not applicable.

Competing interests
M.J.M. received research funding from Bristol-Myers Squibb and travel support from Pierre Fabre. A.S.B. received research support from Daiichi Sankyo, Roche, and honoraria for lectures, consultation or advisory board participation from Roche, Bristol-Meyers Squibb, Merck, Daiichi Sankyo as well as travel support from Roche, Amgen and AbbVie. Z.S. is a former employee of Boehringer

Ingelheim and Turbine AI. M.P. received honoraria for lectures, consultation, or advisory board participation from the following for-profit companies: Bayer, Bristol-Myers Squibb, Novartis, Gerson Lehrman Group (GLG), CMC Contrast, GlaxoSmithKline, Mundipharma, Roche, BMJ Journals, MedMedia, Astra Zeneca, AbbVie, Lilly, Medahead, Daiichi Sankyo, Sanofi, Merck Sharp & Dome, Tocagen. J.N.K declares consulting services for Bioptimus, France; Owkin, France; DoMore Diagnostics, Norway; Panakeia, UK; AstraZeneca, UK; Scailyte, Switzerland; Mindpeak, Germany; and MultiplexDx, Slovakia. Furthermore he holds shares in StratifAI GmbH, Germany, has received a research grant by GSK, and has received honoraria by AstraZeneca, Bayer, Daiichi Sankyo, Eisai, Janssen, MSD, BMS, Roche, Pfizer and Fresenius.

Author details
[1]Division of Oncology, Department of Medicine I, Medical University of Vienna, Waehringer Guertel 18-20, Vienna 1090, Austria
[2]Christian Doppler Laboratory for Personalized Immunotherapy, Department of Medicine I, Medical University of Vienna, Vienna, Austria
[3]Else Kroener Fresenius Center for Digital Health, Medical Faculty Carl Gustav Carus, Technical University Dresden, Dresden, Germany
[4]Precision Medicine Technologies, CBmed GmbH, Graz, Austria
[5]Institute of Medical Statistics, Center for Medical Data Science, Medical University of Vienna, Vienna, Austria
[6]Division of Neuropathology and Neurochemistry, Department of Neurology, Medical University of Vienna, Vienna, Austria
[7]Comprehensive Center for Clinical Neurosciences and Mental Health, Medical University of Vienna, Vienna, Austria
[8]Department of Pathology, Medical University of Vienna, Vienna, Austria
[9]Medical Oncology, National Center for Tumor Diseases (NCT), University Hospital Heidelberg, Heidelberg, Germany
[10]Department of Medicine I, Faculty of Medicine Carl Gustav Carus, University Hospital, Technical University of Dresden, Dresden, Germany

Received: 29 August 2024 / Accepted: 25 January 2025
Published online: 19 February 2025

References

1. Jin MZ, Jin WL (2020) The updated landscape of tumor microenvironment and drug repurposing. Signal Transduct Target Ther 5:166
2. Bader JE, Voss K, Rathmell JC (2020) Targeting metabolism to improve the tumor microenvironment for cancer immunotherapy. Mol Cell 78:1019–1033
3. Bejarano L, Jordão MJC, Joyce JA (2021) Therapeutic targeting of the tumor microenvironment. Cancer Discov 11:933–959
4. Wischnewski V, Maas RR, Aruffo PG et al (2023) Phenotypic diversity of T cells in human primary and metastatic brain tumors revealed by multiomic interrogation. Nat Cancer 4:908–924
5. Yang B, Li X, Zhang W et al (2022) Spatial heterogeneity of infiltrating T cells in high-grade serous ovarian cancer revealed by multi-omics analysis. Cell Rep Med 3:100856
6. Dentro SC, Leshchiner I, Haase K et al (2021) Characterizing genetic intratumor heterogeneity across 2,658 human cancer genomes. Cell 184:2239–2254 e39.
7. Tomasich E, Muhlbacher J, Woran K et al (2024) Immune cell distribution and DNA methylation signatures differ between tumor and stroma enriched compartment in pancreatic ductal adenocarcinoma. Transl Res 271:40–51
8. Biermann J, Melms JC, Amin AD et al (2022) Dissecting the treatment-naive ecosystem of human melanoma brain metastasis. Cell 185:2591–2608 e30.
9. Chevrier S, Levine JH, Zanotelli VRT et al (2017) An immune atlas of clear cell renal cell carcinoma. Cell 169:736–749 e18.
10. Gonzalez H, Mei W, Robles I et al (2022) Cellular architecture of human brain metastases. Cell 185:729–745 e20.
11. Jackson HW, Fischer JR, Zanotelli VRT et al (2020) The single-cell pathology landscape of breast cancer. Nature 578:615–620
12. Karimi E, Yu MW, Maritan SM et al (2023) Single-cell spatial immune landscapes of primary and metastatic brain tumours. Nature 614:555–563
13. Leader AM, Grout JA, Maier BB et al (2021) Single-cell analysis of human non-small cell lung cancer lesions refines tumor classification and patient stratification. Cancer Cell 39:1594–1609 e12.
14. Risom T, Glass DR, Averbukh I et al (2022) Transition to invasive breast cancer is associated with progressive changes in the structure and composition of tumor stroma. Cell 185:299–310 e18.
15. Bankhead P, Loughrey MB, Fernandez JA et al (2017) QuPath: open source software for digital pathology image analysis. Sci Rep 7:16878
16. Shannon CE (1950) Programming a computer for playing chess. Phil Mag 41
17. Jiang K, Parker M, Materi J et al (2023) Epidemiology and survival outcomes of synchronous and metachronous brain metastases: a retrospective population-based study. Neurosurg Focus 55:E3
18. Thomas AJ, Rock JP, Johnson CC et al (2000) Survival of patients with synchronous brain metastases: an epidemiological study in southeastern Michigan. J Neurosurg 93:927–931
19. Bender R, Lange S (2001) Adjusting for multiple testing–when and how? J Clin Epidemiol 54:343–349
20. Pukrop T, Dehghani F, Chuang HN et al (2010) Microglia promote colonization of brain tissue by breast cancer cells in a wnt-dependent way. Glia 58:1477–1489
21. Nozzoli F, Gessi M, Ugolini F et al (2024) Morpho-phenotypic characterization of melanoma brain metastases immune microenvironment: a multicentre retrospective study. EJC Skin Cancer 2
22. Ikarashi D, Okimoto T, Shukuya T et al (2021) Comparison of tumor microenvironments between primary tumors and brain metastases in patients with NSCLC. JTO Clin Res Rep 2:100230
23. Liu JS, Cai YX, He YZ et al (2024) Spatial and temporal heterogeneity of tumor immune microenvironment between primary tumor and brain metastases in NSCLC. BMC Cancer 24:123
24. Ogiya R, Niikura N, Kumaki N et al (2017) Comparison of immune microenvironments between primary tumors and brain metastases in patients with breast cancer. Oncotarget 8:103671–103681
25. Bruni D, Angell HK, Galon J (2020) The immune contexture and immunoscore in cancer prognosis and therapeutic efficacy. Nat Rev Cancer 20:662–680
26. Zhou D, Gong Z, Wu D et al (2023) Harnessing immunotherapy for brain metastases: insights into tumor-brain microenvironment interactions and emerging treatment modalities. J Hematol Oncol 16:121
27. Rauwerdink DJW, Molina G, Frederick DT et al (2020) Mixed response to immunotherapy in patients with metastatic melanoma. Ann Surg Oncol 27:3488–3497

Publisher's note

Springer Nature remains neutral with regard to jurisdictional claims in published maps and institutional affiliations.